Publications of the Astronomical Society of Japan, 2026, **78**(2), 484–492
https://doi.org/10.1093/pasj/psaf156
Advance access publication date: 2026 February 25
Paper

Optimizing infrasound observations for sample return capsule re-entry: Insights from OSIRIS-REx and Hayabusa2

Yasuhiro NISHIKAWA,[1,2,*] Islam HAMAMA,[3] Hany S. ELBEHIRI,[2,3] Yuta HASUMI,[4] Eleonor K. SANSOM,[5] Hadrien DEVILLEPOIX,[6] Masa-yuki YAMAMOTO,[2] and Elizabeth A. SILBER[7]

[1]Division of Math, Sciences, and Information Technology in Education, Osaka Kyoiku University, 4-698-1, Asahigaoka, Kashiwara, Osaka 582-8582, Japan
[2]School of Systems Engineering, Kochi University of Technology, 185 Miyanokuchi, Tosayamada, Kami, Kochi 782-8502, Japan
[3]Egyptian National Data Center, National Research Institute of Astronomy and Geophysics, Helwan, Cairo 11421, Egypt
[4]Graduate School of Engineering, Kochi University of Technology, 185 Miyanokuchi, Tosayamada, Kami, Kochi 782-8502, Japan
[5]Space Science and Technology Centre, Curtin University, GPO Box U1987, Perth, WA 6845, Australia
[6]International Centre for Radio Astronomy Research, Curtin University, GPO Box U1987, Perth, WA 6845, Australia
[7]Sandia National Laboratories, Albuquerque, NM 87123, USA

*Email: nishikawa-y54@cc.osaka-kyoiku.ac.jp

Abstract

The atmospheric entry of meteoroids presents a rare and unpredictable phenomenon, posing challenges for systematic observation and detailed characterization. Such events are nonetheless critical for advancing understanding of acoustic wave propagation, atmospheric structure, and entry dynamics. In contrast, sample return capsules (SRCs) from space missions follow well constrained re-entry trajectories, enabling planned observations of shock wave generation and propagation under controlled conditions. This study compares two SRC atmospheric entries, Hayabusa2 in 2020 and OSIRIS-REx in 2023, to assess how different infrasound array configurations influence shock wave detection and trajectory validation. Hayabusa2's re-entry was monitored using a distributed network of 28 portable infrasound sensors across seven arrays in Woomera, Australia, permitting three-dimensional reconstruction of the trajectory and analysis of wave characteristics. For OSIRIS-REx, a compact four-sensor array deployed near Eureka Airport provided trajectory confirmation through arrival-time differences and back-azimuth estimates. Spectral and waveform analyses revealed differences in signal properties associated with variations in entry angle and velocity. The results illustrate both the strengths and the limitations of the deployed array configurations. The dense and distributed arrays during Hayabusa2's re-entry enabled detailed trajectory reconstruction, whereas the compact array at Eureka primarily provided confirmation of signal coherence and back-azimuth consistency. These case studies highlight that even relatively small arrays, if located close to the predicted ground track, can still capture useful information on arrival direction and timing. Such insights provide practical guidance for planning future observational campaigns of SRC returns and other controlled atmospheric entries, and may also inform approaches to opportunistic observations of meteoroid events and other atmospheric acoustic phenomena.

Keywords: celestial mechanics: orbit determination — meteoroids — space vehicles: atmospheric re-entry — techniques: acoustic

1 Introduction

Asteroids and large meteoroids can serve as natural laboratories when they impact the Earth, as they bring valuable extraterrestrial samples and provide clues about the formation of our solar system. When these objects enter dense regions of the Earth's atmosphere, they generate shock waves (Silber et al. 2018), which eventually decay to infrasound, or low-frequency acoustic waves (Evans and Tempest 1972). Infrasound can propagate over large distances with little attenuation, and as such, it is considered an ideal proxy for detecting impulsive sources in the atmosphere, including volcanoes, lightning, explosions, meteoroids, earthquakes, and re-entry events (ReVelle and Edwards 2007; Arrowsmith et al. 2008; Farges 2009; ElGabry et al. 2017; Pilger et al. 2019; Matoza et al. 2019; Saito et al. 2021; Hamama and Yamamoto 2021; Nishikawa et al. 2022b; Hamama et al. 2022). Observations of meteoroid re-entries contribute to diverse research areas, including the estimation of atmospheric structure, acoustic wave propagation, re-entry physics, and planetary defense. However, objects in the size range of a meter or greater are relatively rare, and because of the stochastic nature of their impact time and location, present a significant challenge in planned observational campaigns, thus limiting opportunities for systematic observation and experimental validation (Silber et al. 2024). To fully characterize the infrasound generation during sample return capsule (SRC) re-entry, it is necessary to understand the fundamental shock wave physics. The formation and propagation of infrasound from atmospheric entries are governed by the entry velocity, entry angle, and fragmentation behavior of the object. For high Mach number entries with limited fragmentation, the resulting shock waves establish an extended, nearly cylindrical source along the trajectory (Silber et al. 2018). The nearly cylindrically expanding shock wave transitions into an acoustic wave. Wind and temperature gradients in the atmosphere may then modify this approximately cylindrical wavefront as it propagates outward. Shallow entry angles further extend the effective source length and strengthen azimuthal directivity (Pilger et al. 2015; Silber2025). While downward-propagating acoustic energy can couple into atmospheric ducts depending on altitude and atmospheric conditions, upward-propagating energy undergoes severe

Received: 2025 October 7; **Accepted:** 2025 December 23

thermospheric attenuation due to molecular diffusion and viscous dissipation (Sutherland and Bass 2004). These propagation characteristics must be accounted for when designing observational strategies and interpreting infrasound signatures from SRCs, space debris, and meteoroid entries. Artificial objects returning to Earth from space, especially SRCs from space exploration missions, follow well known flight trajectories and re-entry dynamics, allowing for planned observations. This predictability presents a unique opportunity to study shock waves and acoustic wave propagation in the atmosphere in detail (Silber et al. 2023).

Previous studies have utilized infrasonic signals from SRC atmospheric re-entries to observe shock waves reaching the ground, which are valuable for trajectory estimation and atmospheric research (Yamamoto et al. 2011; Ishihara et al. 2012; Sansom et al. 2022). For the Japan Aerospace Exploration Agency's (JAXA's) Hayabusa2 SRC on 2020 December 5, 28 portable infrasound sensors (Nishikawa et al. 2024) were deployed across seven observation points. This array successfully estimated the SRC's three-dimensional trajectory and allowed detailed analysis of shock wave propagation through the atmosphere (Nishikawa et al. 2022a). However, deploying such extensive observation arrays is often unfeasible, as SRC flight paths are typically designed to pass over remote deserts or wilderness areas, where access to power and personnel is challenging (Silber et al. 2024).

On 2023 September 24, the National Aeronautics and Space Administration's (NASA's) Origins, Spectral Interpretation, Resource Identification, and Security-Regolith Explorer (OSIRIS-REx) SRC returned to Earth and landed at the Utah Test and Training Range (UTTR). As part of a large multi-institution geophysical observation team, we deployed an array comprising four portable infrasound sensors at Eureka Airport in Nevada to capture infrasonic signals (Silber et al. 2024). Although such a small observation array is limited in its ability to estimate the three-dimensional trajectory, similar to what was done for the Hayabusa2 mission, direct observations beneath the flight path enabled trajectory validation using infrasound signal arrival times and back-azimuth estimates. The use of consistent observational methods across both the Hayabusa2 and OSIRIS-REx missions also enabled a comparative analysis of the shock waves generated by the two SRCs.

This study provides a detailed comparison of the observational data from the OSIRIS-REx and Hayabusa2 SRCs, focusing on how infrasound signal measurements can contribute to three-dimensional trajectory estimation and the analysis of acoustic wave propagation. Furthermore, the impact of the observation array scale on analytical methods and accuracy is explored, offering recommendations for more efficient and effective future observations. By advancing our understanding of acoustic wave propagation mechanisms in the atmosphere, our work aims to improve applications in future artificial object re-entry missions and planetary defense.

2 Methods

2.1 Instrument placement and observations

2.1.1 OSIRIS-REx SRC

In anticipation of the OSIRIS-REx SRC re-entry, four INF04 infrasound sensors were deployed at Eureka Airport, Nevada, in close proximity to the OSIRIS-REx trajectory path, to detect infrasound signals from the shock wave produced by the SRC during the re-entry. The INF04 sensors used during the OSIRIS-REx deployment are condenser-microphone microbarometers with a flat frequency response of 0.1–100 Hz and a minimum detectable pressure of approximately 0.005 Pa. Each unit incorporates MEMS temperature, pressure, and three-axis acceleration sensors, and is equipped with a GNSS receiver for absolute UTC timing. All sensors were operated at a sampling rate of 100 Hz (Nishikawa et al. 2024). Figure 1a shows the location of the infrasound sensors, which were positioned within a few kilometers of the nominal ground track. The array aperture was between 1 and 4 km, allowing measurement of arrival-time differences between the array elements. These timing differences are used to estimate the apparent horizontal phase velocity and arrival azimuth of the wavefront through time-delay analysis, providing constraints on the signal back azimuth and confirming the coherence of the detected signal. Acoustic travel times were calculated assuming straight-line propagation at an average sound speed of 340 m s^{-1} from ground to trajectory altitude. The deployment location was strategically chosen, as the SRC's ground track passed approximately 5 km north of the array at an altitude of 50–60 km during peak aerodynamic heating (Silber et al. 2024; Francis et al. 2024), corresponding to an incidence angle of $\sim 84^\circ$ relative to the horizontal. This made Eureka an optimal site for shock wave detection. Although our array had a small number of sensors, and thus covered a limited geographical area, we optimized the aperture to capture signals generated by the SRC (figure 1a). Further details about our instruments and setup are given by Silber et al. (2024). The overflight occurred at 07:42 Pacific Daylight Time (PDT) (14:42 Universal Time Coordinated (UTC)), under clear morning conditions with sufficient daylight. Although SRCs typically produce bright meteor-like emissions as they descend through the atmosphere, the OSIRIS-REx SRC was not visually observable due to the bright ambient light conditions at the time of re-entry. Nevertheless, an audible component of the associated shock wave was reported at the site. Considering that the OSIRIS-REx SRC re-entered the atmosphere during local morning hours, optical observations for trajectory determination were not feasible.

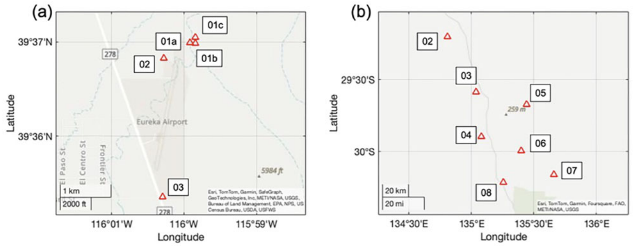

Fig. 1. (a) Infrasound sensor locations for OSIRIS-REx. (b) Infrasound array locations for Hayabusa2.

2.1.2 Hayabusa2 SRC

In contrast to the single-array setup used for OSIRIS-REx, during the Hayabusa2 re-entry on 2020 December 5, seven arrays were deployed across various sites in the Woomera Desert, South Australia. The seven 4-element arrays included a total of 28 INF04 infrasound sensors. The open and flat desert environment enabled greater flexibility in array design, allowing the establishment of a large-scale observation

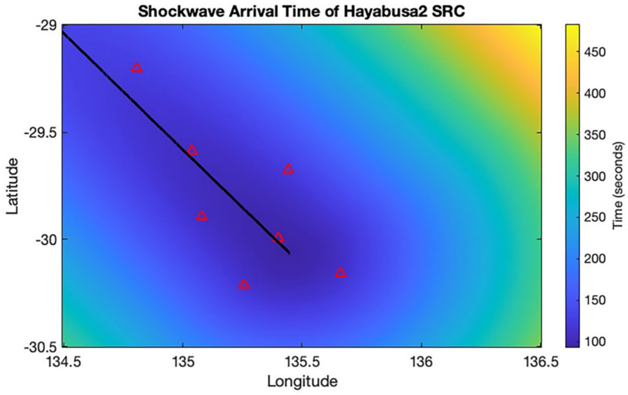

Fig. 2. Arrival time of the infrasound signal (in seconds from 17:30:00 UTC), locations of the infrasound sensors, and trajectory of the Hayabusa2 SRC. The trajectory is estimated from infrasound observations; the SRC moved from northwest to southeast.

network covering a region of approximately 100 km (figure 1b). The network was suitable beneath the predicted trajectory of the SRC, ensuring broad spatial coverage. As the re-entry occurred at 03:28 Australian Central Daylight Time (ACDT), the luminous portion of the fireball trajectory was also visible, enabling integrated visual and acoustic analysis. The multi-modal observational campaign details and instrument setup are given by Sansom et al. (2022). The Hayabusa2 observations used the same INF04 sensor configuration as described for OSIRIS-REx, including the 0.1–100 Hz frequency response, a noise floor of approximately 0.005 Pa, and a 100 Hz sampling rate (Nishikawa et al. 2024). We use the three-dimensional Hayabusa2 SRC trajectory reconstructed by Nishikawa et al. (2022a), which is based on combined infrasound and optical observations.

2.2 Signal analysis

This section describes the signal processing and analysis approaches applied to the infrasound data collected from the OSIRIS-REx and Hayabusa2 SRC re-entry events. Signal arrival times were picked at the first N-wave onset and compared to predicted travel times. For the OSIRIS-REx SRC event, the infrasound sensors were positioned almost directly beneath the re-entry trajectory; thus the signal travel times did not require correction for atmospheric refraction or reflection. The infrasound ray path was assumed to be approximately straight, and its predicted propagation speed was calculated using the average acoustic velocity between the array and the SRC's location (obtained from NASA's nominal trajectory; Francis et al. 2024). The nominal trajectory of the Hayabusa2 SRC was not published. Although the luminous path was optically observed during the nighttime re-entry, the corresponding trajectory data were not made publicly available. Therefore, the trajectory was reconstructed from infrasound observations in that study, and predicted arrival times in this work were calculated based on the infrasound-derived trajectory (figure 2). The frequency content of the infrasound signal provides diagnostic information about the shock wave characteristics associated with hypersonic atmospheric entry; thus, we examined the spectrograms related to both re-entries. Frequency–wavenumber (F–K) analysis, employing Capon's high-resolution estimator on overlapping time windows, yielded estimates of apparent horizontal phase velocity and back azimuth of the incoming signal. Beamforming under a planar-wave assumption provided slowness vectors that further constrained propagation direction and horizontal velocity (Capon 1969).

2.3 Propagation modeling

To assess how infrasound generated by the SRC propagates to far-field distances and to support the development of future geophysical observation strategies for atmospheric re-entries, numerical modeling was conducted using a parabolic equation (PE) approach. The goal of this modeling was not to capture near-field nonlinear shock behavior immediately adjacent to the trajectory, but rather to characterize acoustic energy transmission over larger ranges where linear acoustic approximations are applicable. Atmospheric conditions during the OSIRIS-REx and Hayabusa2 re-entries influence the propagation of infrasonic signals, affecting both transmission losses and arrival characteristics at ground-based sensors. Several numerical methods are available for modeling acoustic propagation, including classical ray-tracing (Georges 1972), normal mode theory (Pierce 1966), and the parabolic equation method (Lingevitch et al. 2002). For this study, the PE method was employed due to its suitability for modeling wave propagation under varying atmospheric conditions, including effects of wind and temperature structure, at far-field distances. By integrating the wide-angle approximation and accounting for high Mach numbers, the PE technique improves efficiency in modeling infrasound propagation (Hamama et al. 2022). The PE solver was developed to include topographic features and an effective sound speed approximation (Waxler et al. 2022), using the ePape module of the NCPAprop package (Waxler et al. 2017). Transmission losses can be estimated using ePape, which identifies the pressure signal amplitude decay between the source and receiver. Several high-resolution numerical wind models can be used to construct detailed wind profiles, which are necessary inputs for infrasound propagation modeling. The Modern-Era Retrospective Analysis for Research and Applications, Version 2 (MERRA-2), provides wind profiles up to altitudes of approximately 80 km. Additionally, the AVOG2S package (Schwaiger et al. 2019) was used to integrate numerical wind observations with empirical models, such as G2S (Drob et al. 2003) and the Horizontal Wind Model 14 (HWM14) (Drob et al. 2015).

For the numerical simulations, PE models were generated to estimate multi-directional propagation behavior for both the Hayabusa2 and OSIRIS-REx events, considering two different assumed source altitudes of 40 and 60 km, respectively. A center frequency of 2 Hz was selected for the simulations, corresponding to the lowest frequency consistently recorded by the infrasound sensors deployed during the observations. Simulations were conducted for a propagation distance of 800 km to assess transmission losses and directional propagation characteristics beyond the immediate vicinity of the trajectory. Atmospheric profiles were constructed up to an altitude of 120 km, incorporating high-resolution wind and temperature data to account for the influence of atmospheric structure on acoustic waveguiding and attenuation. The modeling provides an estimate of how infrasound generated by SRC atmospheric entries would propagate over regional to far-field distances under the prevailing atmospheric conditions at the time of re-entry. The effective sound speed (c_{eff})

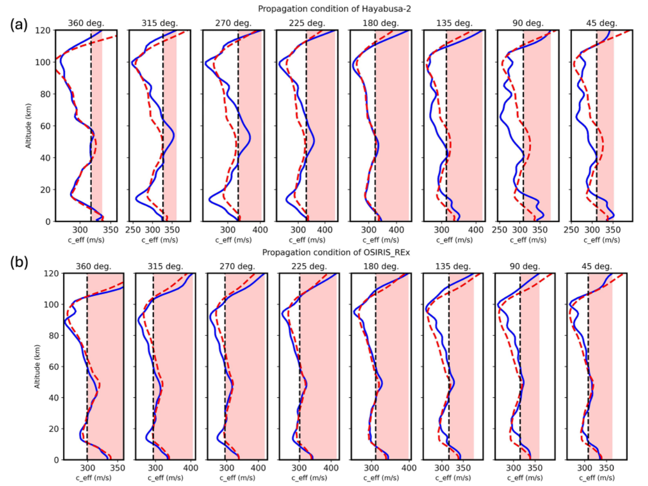

Fig. 3. Comparison of c_{eff} with blue solid lines and c_{th} with dashed red lines for every 45° azimuth to show the propagation conditions in all directions for Hayabusa2. The vertical black dashed line refers the c_{eff} at the altitude.

was used to describe the propagation conditions and can be expressed as

$$c_{\mathrm{eff}}(z) = c_{\mathrm{th}}(z) + u(z) \cdot \sin(\phi) + v(z) \cdot \cos(\phi), \tag{1}$$

where u and v are the zonal and meridional wind speeds, respectively, and ϕ is the azimuth direction of propagation, representing the wind direction. Additionally, the thermodynamic speed c_{th} is given by:

$$c_{\mathrm{th}}(z) = \sqrt{\gamma R T}, \tag{2}$$

where γ is the ratio of specific heats (1.4), and R is the specific gas constant for dry air ($286.9\,\mathrm{J\,kg^{-1}\,K^{-1}}$). The effective sound speeds (c_{eff}) were estimated every 45° azimuth for both events to show the general propagation conditions around the re-entry locations, as shown in figure 3. Ducting of infrasound occurs when the effective sound speed profile exhibits a local maximum with altitude, allowing acoustic energy to become trapped and propagate horizontally over long distances. In the case of Hayabusa2, modeling indicated the presence of a stratospheric duct originating from the southern sector and gradually extending westward, facilitating favorable propagation conditions at lower source altitudes. For the OSIRIS-REx event, the modeling suggested that acoustic energy could couple into both tropospheric and thermospheric ducts, although the dominant contribution to ground-level detections is expected to arise from direct propagation rather than high-altitude ducted returns. Additionally, limited stratospheric ducting was predicted under certain azimuths, depending on the effective sound speed structure relative to the source altitude. These results reflect the sensitivity of long-range infrasound propagation to atmospheric structure, emphasizing the importance of incorporating detailed atmospheric profiles when modeling acoustic wave transmission.

While parabolic equation (PE) modeling provides useful estimates of transmission losses and acoustic propagation behavior at far-field distances, its validity relies on the assumption that the shock waves have sufficiently transitioned to the linear acoustic regime. Accordingly, the modeling conducted in this study was explicitly focused on investigating the far-field propagation characteristics of SRC-generated infrasound, rather than capturing near-field shock dynamics. A simplified representation of the shock source was adopted, assuming a fixed source altitude to characterize propagation behavior over regional distances. In the vicinity of the Eureka Airport array, the SRC trajectory spanned a relatively narrow altitude range, and variations in propagation conditions across this segment are expected to be minor. Therefore, the fixed-altitude approximation is appropriate for assessing far-field transmission trends in this context. It must be recognized, however, that shock wave generation during atmospheric entry evolves continuously along the trajectory, with variations in source altitude, Mach number, and flow conditions as functions of space and time. A full trajectory-resolved modeling approach, discretizing the entry path into a series of evolving source points, would be required to accurately reconstruct the spatiotemporal evolution of the infrasound field. The far-field propagation modeling presented here serves as an exploratory analysis intended to support the development of optimized geophysical observation strategies for future SRC missions, space debris re-entries, and atmospheric entry phenomena.

3 Results

3.1 Analysis of infrasound from SRC re-entry events

This section describes the infrasound signals generated by the atmospheric entries of Hayabusa2 and OSIRIS-REx, based on our ground-based array observations.

3.1.1 OSIRIS-REx

Despite the proximity of the array to the trajectory, the *F–K* method was effective in resolving the wave parameters, confirming the signal coherence and directionality. In addition to our deployment at Eureka Airport, Kc et al. (2025) reported infrasound observations of the OSIRIS-REx SRC re-entry from Wendover Airport, located approximately 220 km east of our site. These independent observations also showed arrival times and back azimuths consistent with the NASA-provided trajectory, indicating that the nominal trajectory remained accurate at long range. Figure 4 shows the combined waveform, which illustrates the time differences between the four sensors. These time differences are highly relevant for data analysis, as they reflect the varying shock wave arrival times at the different sensors. When comparing the predicted signal arrival time with the observed times from the infrasound sensors, the uncertainty was within 0.3 s (table 1). The small arrival-time difference indicates that the actual trajectory of the SRC closely matched the nominal trajectory. However, as the observation point moves farther from the trajectory (far-field), the influence of horizontal winds, along with the effects of atmospheric refraction and reflection, becomes more significant, and can cause a nonnegligible difference between the calculated and observed arrival times. Therefore, at long-range, a simple straight-path approximation might no longer hold.

The waveform shows a high degree of similarity across all sensors. The signals are recorded as N-waves, which are characteristic of the shock wave generating source (Plotkin 2002). The sensors recorded positive phase overpressure values ranging from 1.7 to 2.25 Pa, followed by a sharp underpressure trough with absolute values between 1 and 1.25 Pa. The signal

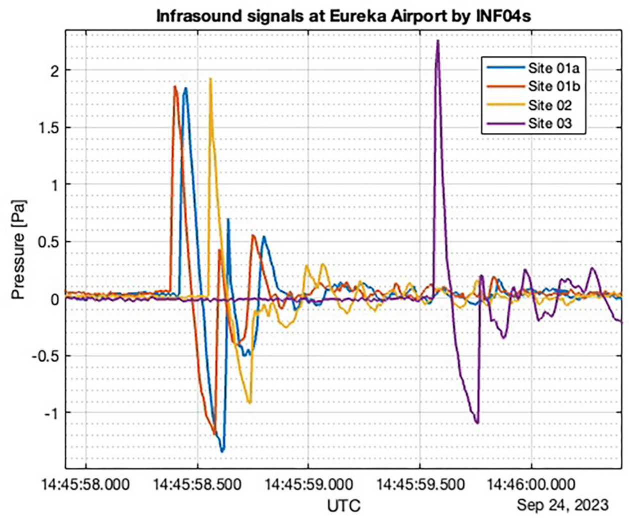

Fig. 4. Combined waveforms for the four sensors detecting the OSIRIS-REx re-entry.

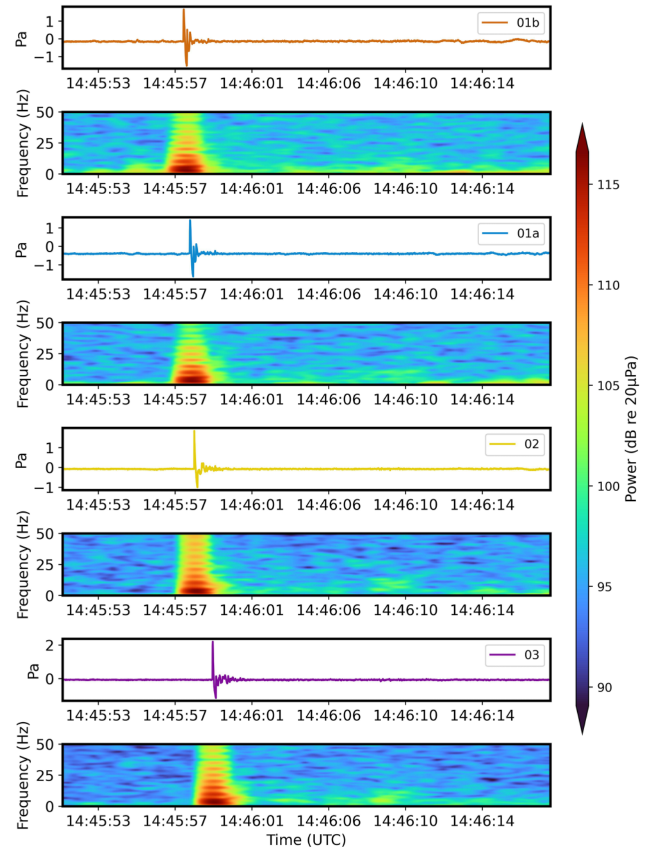

Fig. 5. Time series and spectrograms for each infrasound sensor. The time-series waveforms are arranged according to arrival time, from the earliest to the latest. The spectrograms show the temporal distribution of frequency content detected by each sensor.

corresponds to the direct arrival of infrasound signals generated by the SRC passing through the atmosphere.

Figure 5 shows the waveforms and corresponding spectrograms, illustrating the frequency content detected by the four sensors. Most of the energy is confined to low frequencies, mostly below 20 Hz.

The results of the *F*–*K* analysis, shown in figures 6 and 7, indicate a short burst of high power coherency lasting several seconds starting around 14:46:00 UTC. The infrasound wave propagates with an apparent velocity of 2236 m s^{-1} and a back azimuth of 26 degrees. The dashed line in the azimuth panel represents the approximate direction associated with ballistic shock arrival, located to the north and slightly east of the infrasound detection site. The high value of trace velocity indicates a high-altitude source, consistent with the OSIRIS-REx overflight.

Considering that the OSIRIS-REx SRC re-entered the atmosphere during the morning local time, optical observations for trajectory determination were not conducted. Infrasound sensors were placed almost directly beneath the SRC's trajectory; thus the arrival times of the shock waves did not require adjustments for atmospheric refraction or reflection. The shock wave path was to be straight, and its speed was calculated using the average value from the ground to the altitude of the trajectory. This study focuses exclusively on atmospheric infrasonic waves, which propagate at acoustic speeds that vary significantly with altitude—from values below 330 m s^{-1} near the tropopause to more than 350 m s^{-1} near the surface, after leaving the shock front, and can be detected by ground-based infrasound arrays. The infrasound arrival time was calculated based on NASA's nominal trajectory (Francis et al. 2024). A comparison between the predicted and observed arrival times is shown in figure 8, indicating uncertainties within 0.3 s for all Eureka stations (table 1). These small residuals demonstrate that the actual SRC trajectory closely matched the pre-planned nominal path. At greater ranges, however, atmospheric winds and refraction effects can introduce larger deviations between calculated and observed arrival times, although such effects were negligible for the near-field Eureka observations.

3.2 Hayabusa2

Comparative analysis of the Hayabusa2 SRC and similar re-entry events provides robust constraints on source characteristics and demonstrates the utility of infrasound for monitoring both artificial and natural atmospheric entries. The 28-sensor network recorded signals from 0.5 up to 50 Hz, with Hayabusa2 SRC exhibiting a slightly lower dominant frequency range compared to OSIRIS-REx, likely reflecting differences in capsule size and entry velocity. Proximity to the

Table 1. Sensor locations and infrasound signal arrival times.*

Label	Latitude	Longitude	Altitude (m)	Arrival time obs (UTC)	Arrival time calc (UTC)
01a	39.6166	−115.9986	1802	14:45:58.4	14:45:58.6
01b	39.6165	−115.9974	1802	14:45:58.4	14:45:58.6
02	39.6138	−116.0046	1803	14:45:58.6	14:45:58.8
03	39.5893	−116.0049	1810	14:45:59.6	14:45:59.9

*Columns 5 and 6 list observed and predicted signal arrival times, respectively.

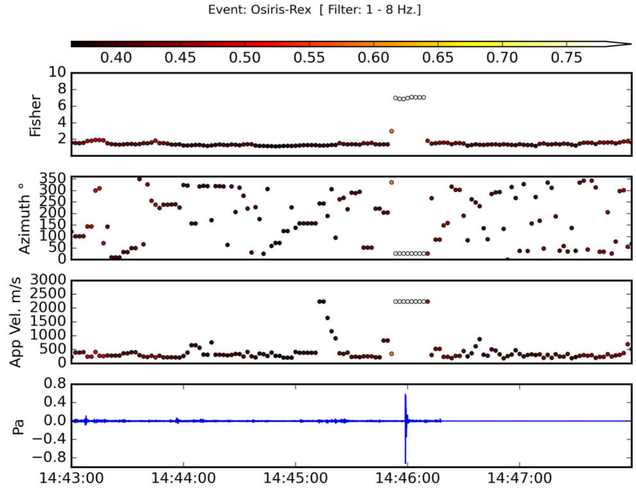

Fig. 6. Results of the *F*–*K* analysis for the OSIRIS-REx event. The panels show, from top to bottom, the Fisher statistics, back azimuth, apparent horizontal velocity, and the filtered infrasound waveform. These quantities exhibit coherent behavior only for a few seconds around 14:46 UTC.

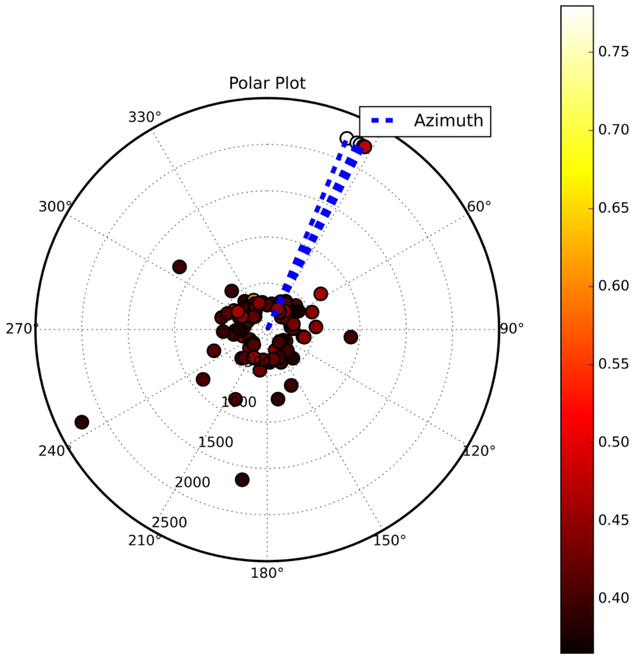

Fig. 7. A polar plot showing the distribution of back azimuth estimated from the *F*–*K* analysis, with points clustered around the dominant direction consistent with the OSIRIS-REx SRC trajectory.

source posed analytical challenges, but *F*–*K* analysis nevertheless revealed array-dependent variations in back azimuth, consistent with treating the SRC as a moving line source rather than a point source emitter (Silber 2025). Figures 9a and 9b show the analysis of filtered waveforms (2–8 Hz) for two representative arrays: Jacob's Bore (figure 1b, site 08), located west of the Hayabusa2 trajectory, and the Twins array (figure 1b, site 06), positioned directly beneath it. The corresponding polar plots (figures 9c and 9d) indicate back azimuths of 0° to 5° for Jacob's Bore and 320° to 325° for the Twins array, in agreement with the known flight azimuth. A comparison between predicted and observed arrival times (figure 2) shows timing residuals within ±2 s at all but one

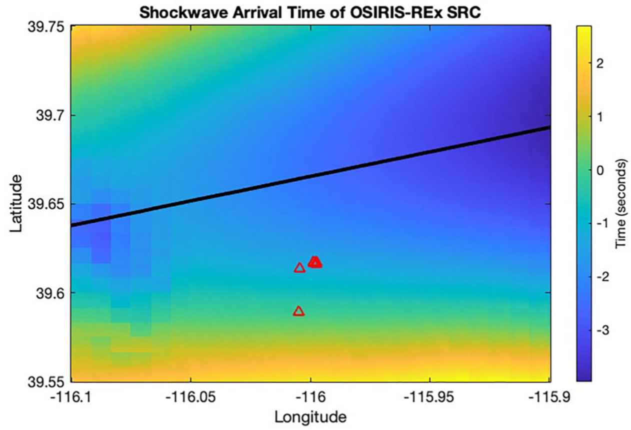

Fig. 8. Arrival time of the shock wave (in seconds after 14:46:00 UTC), location of the infrasound sensors, and trajectory of the SRC; the SRC moved from west to east and the shock wave propagated from east to west in the form of a parabola. Height data are applied for each cell.

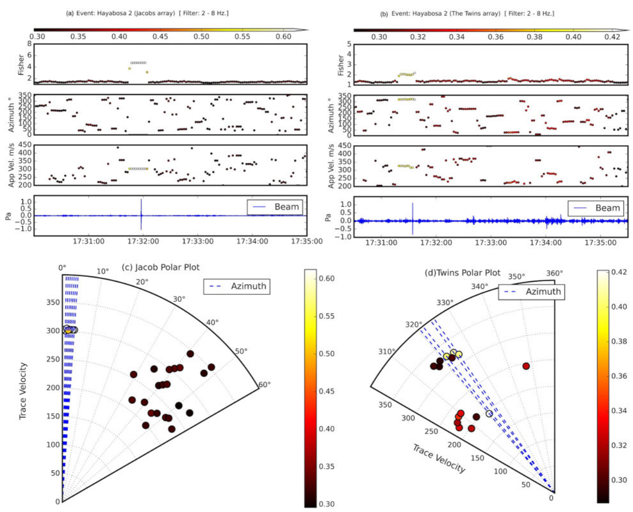

Fig. 9. (a) *F*–*K* analysis for Hayabusa2 for the Jacob's Bore array. (b) The *F*–*K* analysis for the Twins array. (c) Polar plots referring to the Hayabusa2 re-entry shock wave for the Jacob's Bore array. (d) Polar plots for the Twins array.

site (19 s discrepancy at site 08) (table 2). This outlier likely reflects continued infrasound generation beyond the visible-light phase. Therefore, by deploying large-scale infrasound arrays near the end of the SRC's trajectory, it may be possible to determine the trajectory in greater detail than through optical observations alone.

3.3 Far-field propagation modeling outcomes

Ducting of infrasound occurs when the effective sound speed profile exhibits a local maximum with altitude, allowing acoustic energy to become trapped and propagate horizontally over long distances. In the case of Hayabusa2, modeling indicated the presence of a stratospheric duct originating from the southern sector and gradually extending westward, facilitating favorable propagation conditions at lower source altitudes. For the OSIRIS-REx event, the modeling suggested that acoustic energy could couple into both tropospheric and thermospheric ducts, although the dominant contribution to

Table 2. Sensor locations and infrasound signal arrival times for Hayabusa2.*

Label	Latitude	Longitude	Altitude (m)	Arrival time obs (UTC)	Arrival time calc (UTC)
02	−29.20251	134.80632	171	17:32:05	17:32:07
03	−29.58604	135.03752	203	17:31:47	17:31:48
04	−29.89498	135.08017	200	17:31:40	17:31:39
05	−29.67463	135.44238	223	17:32:03	17:32:05
06	−29.99510	135.39998	200	17:31:34	17:31:34
07	−30.15792	135.66090	200	17:31:34	17:31:53
08	−30.21261	135.25473	178	17:31:59	17:31:57

*Columns 5 and 6 list observed and predicted signal arrival times, respectively.

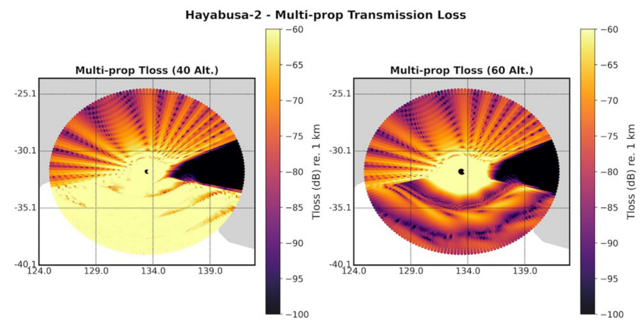

Fig. 10. Multi-propagation transmission loss estimations for 2 Hz frequency around Hayabusa2 for a range up to 800 km with two different assumptions of the shock wave altitudes at 40 and 60 km, respectively.

ground-level detections is expected to arise from direct propagation rather than high-altitude ducted returns. Additionally, limited stratospheric ducting was predicted under certain azimuths, depending on the effective sound speed structure relative to the source altitude. These results reflect the sensitivity of long-range infrasound propagation to atmospheric structure, emphasizing the importance of incorporating detailed atmospheric profiles when modeling acoustic wave transmission.

Far-field transmission losses were modeled at 2 Hz for assumed source altitudes of 40 and 60 km. At 40 km altitude, the transmission losses were almost below −60 dB in the southern area from the shock wave, suggesting that infrasound signals could be detected in this area if infrasound arrays were deployed. However, when the source altitude was increased to 60 km, the duct became weaker in the same region, as shown in figure 10. These results emphasize the critical role of source altitude and array placement in designing future infrasound networks for re-entry and bolide observations.

4 Discussion

The comparative analysis of the OSIRIS-REx and Hayabusa2 SRC re-entries provides a framework for evaluating the effects of shock source characteristics, entry geometry, and observational network configuration on infrasound detectability. Both events involved the formation of radially propagating shock fronts associated with hypersonic flow, resulting in an extended, nearly cylindrical line source geometry aligned along the trajectory (Silber 2025). As the initially nonlinear shocks decayed into the infrasonic regime, the cylindrical source morphology was preserved, resulting in spatially anisotropic acoustic radiation concentrated along the trajectory axis (Silber et al. 2018).

For the OSIRIS-REx SRC, the combination of a shallow entry angle and high Mach number is expected to have produced a coherent series of radially expanding shocks, generating classical N-wave signatures recorded by the infrasound array deployed near Eureka Airport. The observed waveform structures are consistent with the expected acoustic signatures characteristic of weakly decayed cylindrical shocks (ReVelle 1976). Based on the observed trajectory geometry and the limited altitude span traversed near the array, the infrasound signal arrivals are expected to exhibit ballistic propagation consistent with theoretical expectations (ReVelle and Edwards 2007) and supported by recent observational studies. The minor differences between predicted and observed arrival times are consistent with the reconstructed entry, descent, and landing (EDL) trajectory estimated post-entry (Francis et al. 2024). The lower shock generation altitude associated with Hayabusa2 (∼40 km) compared to OSIRIS-REx (∼60 km) likely increased the coupling of acoustic energy into stratospheric ducts, thus increasing the potential detection distances under favorable atmospheric conditions. Nonetheless, for both events, the principal mechanism governing signal arrival near the trajectory is expected to be direct propagation from the source region, with thermospheric returns contributing negligibly due to strong dissipative losses at higher altitudes. Variations in atmospheric effective sound speed associated with horizontal winds and thermal structure introduce secondary modulations to propagation conditions but do not fundamentally alter the prevailing ballistic propagation regime under the observed entry scenarios.

The observational strategies implemented for these two re-entry events clearly illustrate the dependence of trajectory analysis capabilities on infrasound array configuration. The Hayabusa2 campaign employed a widely distributed sensor network, enabling robust three-dimensional trajectory reconstruction through multi-station back-azimuth and arrival-time analyses. In contrast, the OSIRIS-REx deployment relied upon a spatially compact, single-array approach, which, while insufficient for full trajectory reconstruction, proved effective for trajectory validation based on local arrival-time gradients and back-azimuth estimation directly beneath the flight path. This comparison emphasizes the critical importance of aligning array configuration with specific mission objectives, whether prioritizing comprehensive spatial coverage or detailed near-field source characterization.

Modeling results and observations from both missions demonstrate the central role of shock wave altitude, array geometry, and atmospheric conditions in influencing the detectability and interpretability of hypersonic re-entry signatures. Notably, in rare cases, thermospheric or upper-atmospheric arrivals of meteoroid-generated infrasound have been observed at regional distances (Ott et al. 2021; Silber 2024); however, such arrivals were not prominently observed during the SRC events examined in this study, indicating that direct ballistic propagation was the dominant mode of acoustic transmission for these re-entry scenarios.

The methodologies and analytical approaches developed through these SRC re-entry observations offer direct applicability to future atmospheric entry scenarios, including controlled spacecraft returns, natural bolide events, and orbital debris re-entries. Strategically designed infrasound arrays, optimized with respect to expected shock intensity, entry geometry, anticipated atmospheric conditions, and logistical constraints, can significantly advance our understanding of high-altitude shock phenomena and improve global infrasound monitoring capabilities relevant to planetary defense and geophysical studies. Although this study employed simplified propagation modeling and a limited sensor deployment strategy, the findings align well with the broader physical understanding established through previous trajectory-resolved analyses of atmospheric entry phenomena. Ultimately, future infrasound observation campaigns will greatly benefit from integrated multi-array networks coupled with sophisticated propagation modeling to achieve detailed, spatially resolved characterization of atmospheric entry events and their associated infrasonic signals.

5 Conclusion

This study demonstrates the utility of portable infrasound sensors for the detection and characterization of shock waves generated by sample return capsule (SRC) atmospheric re-entries. Comparative analyses of the OSIRIS-REx and Hayabusa2 observation campaigns provided an evaluation of how array scale and configuration impact trajectory reconstruction capabilities. The extensive, multi-station array deployed for Hayabusa2, covering approximately 100 km, enabled comprehensive trajectory determination (Nishikawa et al. 2022a) through back-azimuth and arrival-time analyses across spatially distributed stations. Conversely, the spatially compact array used during the OSIRIS-REx event, positioned directly beneath the nominal trajectory, provided sufficient spatial resolution to confirm the pre-entry trajectory but lacked the aperture necessary for full three-dimensional trajectory estimation.

The altitude at which shock waves are generated critically influenced infrasound detectability and propagation conditions. For OSIRIS-REx, with a shock source altitude near 60 km, direct arrivals were reliably recorded close to the ground track, whereas increased acoustic attenuation and less favorable coupling into stratospheric ducts diminished signal detectability at greater distances. In contrast, the lower shock generation altitude (∼40 km) of the Hayabusa2 SRC likely enhanced acoustic energy transmission into stratospheric ducts, extending the potential detection range under conducive atmospheric conditions. Despite these differences, observational coverage for both missions remained primarily confined to regions proximal to the respective trajectories due to array deployment strategies.

This analysis demonstrates that the effectiveness of infrasound monitoring for atmospheric entry events is strongly dependent on array geometry, scale, and shock generation altitude. Propagation modeling, including the calculation of transmission losses and the characterization of effective sound speed structures, is indispensable for informing optimal sensor placement relative to expected trajectory parameters. Moreover, accurate representation of atmospheric conditions, including detailed wind profiles and thermal stratification, is necessary to improve the predictive capabilities of propagation modeling and improve the interpretation of recorded infrasound signals.

The methodologies and analytical considerations presented here provide essential guidance for future infrasound-based observation campaigns of atmospheric entry phenomena. Distributed sensor networks facilitate comprehensive trajectory reconstruction, while strategically located compact arrays positioned beneath projected trajectories can deliver critical local trajectory validation. Future observational efforts should integrate infrasound data with complementary observational modalities, including optical and radar measurements, to obtain a comprehensive understanding of atmospheric re-entry dynamics. The observational strategies and modeling methodologies described in this work contribute substantially to the advancement of global monitoring frameworks for SRC returns, space debris re-entries, and natural bolide phenomena.

Data and resources

NCPAProp is an open software package available on GitHub ⟨https://github.com/chetzer-ncpa/ncpaprop-release⟩. The Fortran 90 source code for the AVO-G2S model is freely available at ⟨https://github.com/usgs/volcano-avog2s⟩. The wind datasets were extracted from the Modern-Era Retrospective Analysis for Research and Applications, version 2 (MERRA-2), available at ⟨https://disc.gsfc.nasa.gov/⟩. Infrasound data are not publicly available at this time, but can be obtained on a case-by-case basis by contacting the corresponding author.

Conflicts of interest

The authors declare that there are no conflicts of interest associated with this study.

Funding

This research was primarily supported by the Murata Science Foundation (grant number M20AN115) and the NEXCO Group Companies' Support Fund for Disaster Prevention Measures on Expressways. Additional support was provided by the Australian Research Council (grant DP200102073) through the Desert Fireball Network team. Travel and instrumentation funding were supported by the Institute of Geoscience Research and the Curtin Faculty of Science and Engineering. This work was also supported by a designated donation from Yugen Kaisha Asakura Dojo (Asakura Dojo LLC) to Kochi University of Technology for the project "Development of Observation Devices for Antarctic Use and Infrasound Seismology of Icy Bodies" (2024 August–2025 March).

Acknowledgments

The authors gratefully acknowledge the Board of Eureka County Commissioners and the personnel at Eureka Municipal Airport. Although the team from Japan was unable to travel to Australia due to COVID-19 restrictions, the observation of the Hayabusa2 SRC re-entry was made possible through the efforts of volunteers. We extend our heartfelt thanks to Geoffrey Bonning, Andrew Cool, Karen Donaldson, Glyn Donaldson, Michael Roche, and Terrence Wardle for their invaluable support, without which this study would not have been completed. We also wish to express our gratitude to the Hayabusa2 Project Team at JAXA.

The authors made extensive use of the Python packages Matplotlib,[1] ObsPy (Beyreuther et al. 2010), and NumPy (Harris et al. 2020). We thank all institutions and researchers involved in providing the observational data used in this study. Special thanks go to the Woomera Test Range, particularly Guy Mold and Colin Telfer, as well as the Defence Science and Technology Group, especially Kruger White and the team.

This article has been authored by an employee of National Technology & Engineering Solutions of Sandia, LLC under Contract No. DE-NA0003525 with the US Department of Energy (DOE). The employee owns all right, title, and interest in and to the article and is solely responsible for its contents. The United States Government retains and the publisher, by accepting the article for publication, acknowledges that the United States Government retains a non-exclusive, paid-up, irrevocable, world-wide license to publish or reproduce the published form of this article or allow others to do so, for United States Government purposes. The DOE will provide public access to these results of federally sponsored research in accordance with the DOE Public Access Plan ⟨https://www.energy.gov/downloads/doe-public-access-plan⟩. Any subjective views or opinions that might be expressed in the paper do not necessarily represent the views of the US Department of Energy or the United States Government.

References

Arrowsmith, S. J., et al. 2008, Geophysical J. Int., 175, 291
Beyreuther, M., Barsch, R., Krischer, L., Megies, T., Behr, Y., & Wassermann, J. 2010, Seismological Res. Lett., 81, 530
Capon, J. 1969, Proc. IEEE, 57, 1408
Drob, D. P., et al. 2015, Earth Space Sci., 2, 301
Drob, D. P., Picone, J. M., & Garcés, M. 2003, J. Geophysical Res., 108, 4680
ElGabry, M. N., Korrat, I. M., Hussein, H. M., & Hamama, I. H. 2017, J. Astron. Geophysics, 6, 68
Evans, M. J., & Tempest, W. 1972, J. Sound Vibration, 22, 19
Farges, T. 2009, in Lightning: Principles, Instruments and Applications, ed. H. D. Betz et al. (Dordrecht: Springer), 417
Francis, S. R., Johnson, M. A., Queen, E., & Williams, R. A. 2024, NASA Technical Reports Server, ID 20240000629
Georges, T. M. 1972, J. Acoustical Soc. America, 51, 206
Hamama, I., et al. 2022, J. Acoustical Soc. America, 151, 1575
Hamama, I., & Yamamoto, M. 2021, Sensors, 21, 894
Harris, C. R., et al. 2020, Nature, 585, 357
Ishihara, Y., Hiramatsu, Y., Yamamoto, M., Furumoto, M., & Fujita, K. 2012, Earth Planets Space, 64, 655
Kc, R. J., Wilson, T. C., Fox, D., Spillman, K. B., Garcés, M. A., & Elbing, B. R. 2025, Seismological Res. Lett., 96, 2753
Lingevitch, J. F., Collins, M. D., Dacol, D. K., Drob, D. P., Rogers, J. C. W., & Siegmann, W. L. 2002, J. Acoustical Soc. America, 111, 729
Matoza, R. S., Fee, D., Green, D., & Mialle, P. 2019, in Infrasound Monitoring for Atmospheric Studies: Challenges in Middle Atmosphere Dynamics and Societal Benefits, ed. L. Pichon et al. (Cham: Springer), 1023
Nishikawa, Y., et al. 2022a, PASJ, 74, 308
Nishikawa, Y., Yamamoto, M., Nakajima, K., Hamama, I., Saito, H., Kakinami, Y., Yamada, M., & Ho, T.-C. 2022b, Sci. Rep., 12, 22354
Nishikawa, Y., Yamamoto, M., Yokota, A., Hasumi, Y., & Hamajima, G. 2024, Discover Geoscience, 2, 82
Ott, T., et al. 2021, A&A, 654, A98
Pierce, A. D. 1966, J. Acoustical Soc. America, 39, 1139
Pilger, C., Ceranna, L., Ross, J. O., Le Pichon, A., Mialle, P., & Garcés, M. A. 2015, Geophysical Res. Lett., 42, 2523
Pilger, C., Gaebler, P., Ceranna, L., Le Pichon, A., Vergoz, J., Perttu, A., Tailpied, D., & Taisne, B. 2019, Nat. Hazards Earth Syst. Sci., 19, 2811
Plotkin, K. J. 2002, J. Acoustical Soc. America, 111, 530
Revelle, D. O. 1976, J. Geophysical Res., 81, 1217
Revelle, D. O., & Edwards, W. N. 2007, Meteoritics Planetary Sci., 42, 271
Saito, H., Yamamoto, T., Nakajima, K., Kuramoto, K., & Yamamoto, M. 2021, J. Acoustical Soc. America, 149, 591
Sansom, E. K., et al. 2022, PASJ, 74, 50
Schwaiger, H. F., Iezzi, A. M., & Fee, D. 2019, Comput. Geoscience, 125, 90
Silber, E. A. 2024, Remote Sensing, 16, 3628
Silber, E. A. 2025, Abstract, Proc. EGU General Assembly 2025, id. EGU25-4030
Silber, E. A., et al. 2024, Planetary Sci. J., 5, 213
Silber, E. A., Boslough, M., Hocking, W. K., Gritsevich, M., & Whitaker, R. W. 2018, Advances Space Res., 62, 489
Silber, E. A., Bowman, D. C., & Albert, S. 2023, Atmosphere, 14, 1473
Sutherland, L. C., & Bass, H. E. 2004, J. Acoustical Soc. America, 115, 1012
Waxler, R. M., Assink, J. D., Hetzer, C., & Velea, D. 2017, J. Acoustical Soc. America, 141, 3627
Waxler, R., Hetzer, C. H., Assink, J. D., & Blom, P. 2022, J. Acoustical Soc. America, 152, 3659
Yamamoto, M., Ishihara, Y., Hiramatsu, Y., Kitamura, K., Ueda, M., Shiba, Y., Furumoto, M., & Fujita, K. 2011, PASJ, 63, 971

[1] J. D. Hunter & D. Dale, Matplotlib 0.90.0 User's Guide (Matplotlib Development Team, Chicago, IL, 2007) ⟨https://matplotlib.org/⟩.

Received: 2025 October 7; Accepted: 2025 December 23